physics

MDPI

Communication

Charm Quark Evolution in the Quark–Gluon Plasma with Various Quark Contents

Valeriya Mykhaylova

Institute of Theoretical Physics, Jagiellonian University, ul. prof. St. Łojasiewicza 11, 30-348 Kraków, Poland; valeriya.mykhaylova@uj.edu.pl

Abstract

The production rate of charm quarks in strongly interacting matter is investigated under various conditions, employing the effective quasiparticle framework. This phenomenological approach treats quarks and gluons as quasiparticles with dynamically generated self-energies linked to the medium. This paper studies thermal production of charm quarks in hot deconfined matter when those quarks are treated as impurities with a constant mass or as dynamical quarks dressed by the effective mass. When charm quarks are considered quasiparticles, their large (compared to the bare value) mass generates a significant decrease in the production rate in the crossover region. Various initial conditions for the evolution of the system are applied, showing that lower initial temperature leads to the continual suppression of the charm quark production rate, which appears in line with the previously reported estimate at certain values of the initial parameters.

Keywords: charm quark; heavy flavor; kinetic theory in nuclear collisions; quark–gluon plasma; quasiparticles; QCD phenomenology; heavy ion collisions

1. Introduction

For several decades, observables related to heavy quarks, in particular to charm c-quarks, have been considered exceptional probes of the phenomena occurring in heavy ion collisions; for a recent comprehensive review, see [1]. The physics of heavy quarks has been extensively studied both experimentally [2–4] and theoretically [5–10].

This paper analyzes the thermal production rate of charm quarks in strongly interacting matter with various quark contents. Alongside the commonly used description of the quark–gluon plasma (QGP) with the number of quark flavors $N_f = 2+1$ (of two light quarks and the strange quark), additionally a system with equilibrated charm quarks, i.e., the $N_f = 2+1+1$ case, is investigated. The calculations are performed in the well-grounded quasiparticle model (QPM), which allows one to investigate the dynamical properties of hot QCD matter with thermodynamics obtained from the state-of-the-art lattice quantum chromodynamics (lQCD). The QPM effectively connects perturbative and non-perturbative QCD regimes, therefore allowing for calculation of various QGP parameters in a wide range of temperatures. Previous successes of the considered model include, among others, the computation of transport coefficients, such as shear or bulk viscosities, which appeared in line with the results obtained from other formalisms [11–13].

Various characteristics of heavy quarks have been recently explored in the alternative quasiparticle approaches [14,15], including the extension of the system to $N_f = 2+1+1$ quark flavors. However, the production rate of charm quasiquarks has not been discussed in the literature so far. Moreover, although the effective models [11,14,15] are based on the

check for updates

Received: 1 June 2025
Revised: 15 July 2025
Accepted: 21 July 2025
Published: 5 September 2025

Citation: Mykhaylova, V. Charm Quark Evolution in the Quark–Gluon Plasma with Various Quark Contents. *Physics* **2025**, *7*, 39. https://doi.org/10.3390/physics7030039

Copyright: © 2025 by the author. Licensee MDPI, Basel, Switzerland. This article is an open access article distributed under the terms and conditions of the Creative Commons Attribution (CC BY) license (https://creativecommons.org/licenses/by/4.0/).

same concept, their main features, such as the quasiparticle masses or coupling, are defined differently, and this study additionally illustrates the influence of the model assumptions.

The structure of the paper is as follows. Section 2 introduces the basic components of the QPM, focusing on the differences between the effective running coupling and the quasiparticle masses in the $N_f = 2+1$ and $N_f = 2+1+1$ cases. Section 3 presents the production rate of charm quarks in the QGP with different quark contents. It additionally discusses how the production rate depends on the initial conditions of the one-dimensional expansion of the ideal fluid by comparing the results obtained earlier from a different quasiparticle framework [16]. The conclusions are given in Section 4.

2. Quasiparticle Model

The QPM is based on the assumption that the QGP consists of quasiparticles, i.e., dynamical quarks and gluons, which are characterized by their effective masses [11]

$$m_i(G(T),T) = \sqrt{\left(m_i^0\right)^2 + \Pi_i(G(T),T)}, \tag{1}$$

with $i = g, l, s, (c)$ denoting quasigluons, light (degenerate up and down), strange, and charm quarks, respectively, and m_i^0 their current masses. Here, $m_l^0 = 5$ MeV, $m_s^0 = 95$ MeV, and $m_c^0 = 1.3$ GeV are used, while bare gluons are naturally massless, $m_g^0 = 0$. Note that the c-quarks are treated as quasiparticles in the case of $N_f = 2+1+1$ only, while in the $N_f = 2+1$ case, the charm quarks retain their current mass.

The effective masses are acquired through the dynamically generated self-energies Π_i emerging from strong interactions within the deconfined medium [17],

$$\Pi_g(G(T),T) = \left(3 + \frac{N_f}{2}\right)\frac{G^2(T)}{6}T^2, \tag{2}$$

$$\Pi_{l,s,(c)}(G(T),T) = 2\left(m_{l,s,(c)}^0\sqrt{\frac{G^2(T)}{6}T^2} + \frac{G^2(T)}{6}T^2\right), \tag{3}$$

where $G(T)$ is the effective running coupling and T is the temperature. In Equations (2) and (3), the self-energies are defined at vanishing chemical potential, $\mu = 0$ and N_f in Equation (2) equals 3 or 4, depending on whether the c-quarks are treated as impurities or as quasiparticles, on a par with other QGP constituents.

Figure 1 shows the effective running coupling $G(T)$ deduced from the lQCD results for the entropy density of the QGP with $N_f = 2+1$ [18] and $N_f = 2+1+1$ [19] quark flavors. The uncertainties are transferred from the original errors of the lattice data. The charm quarks start to contribute to the equation of state for $T \gtrsim 300$ MeV [19]. Therefore, at lower temperatures, the couplings for different N_f overlap due to the identical entropy densities of the systems. At high temperatures, one observes that in the presence of dynamical charm quarks, the $G(T)$ decreases compared to the running coupling for $N_f = 2+1$.

Figure 2 compares the dynamical masses of the quasiparticles in the QGP with different quark contents. In the case of $N_f = 2+1$, c-quarks enter the system as impurities of constant mass $m_c = 1.3$ GeV, with no contribution to the QGP thermodynamics. Alongside, a full quasiparticle picture is considered in which all the QGP constituents, including charm quarks, are treated as dynamical degrees of freedom in thermal equilibrium. Note that such a description is more consistent since it properly accounts for strong interactions transferred from the lQCD results to the QPM through the effective coupling and the medium-dependent masses of all quasiparticle species.

The temperature dependence of the presented masses is defined by Equations (1)–(3). Apart from charm quarks, whose bare mass m_c^0 in the $N_f = 2+1+1$ scenario considerably

dominates the dynamical part of m_c, one observes that the self-energy Π_i provides dominant contributions to the effective masses of the quasiparticles. Also, similar to the behavior of the coupling, the most pronounced difference in the $N_f = 2+1$ and $N_f = 2+1+1$ cases is observed for temperatures above 300 MeV, at which charm quarks enter the QGP equation of state [19].

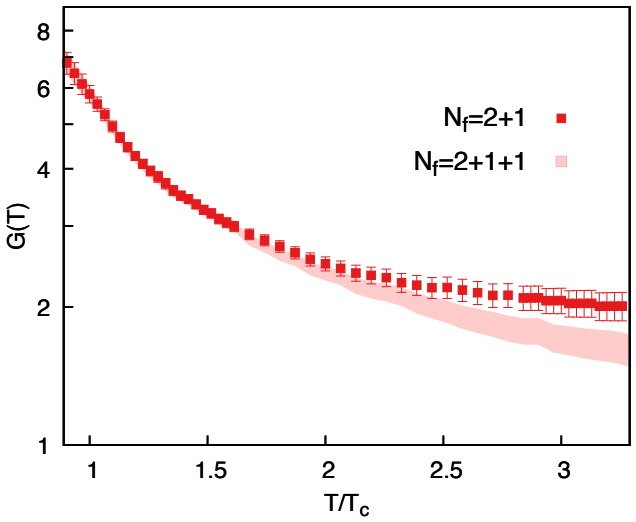


Figure 1. Effective running coupling $G(T)$, as a function of temperature T scaled by the pseudocritical value $T_c = 155$ MeV, for systems with different numbers N_f of quark flavors (see text for details).

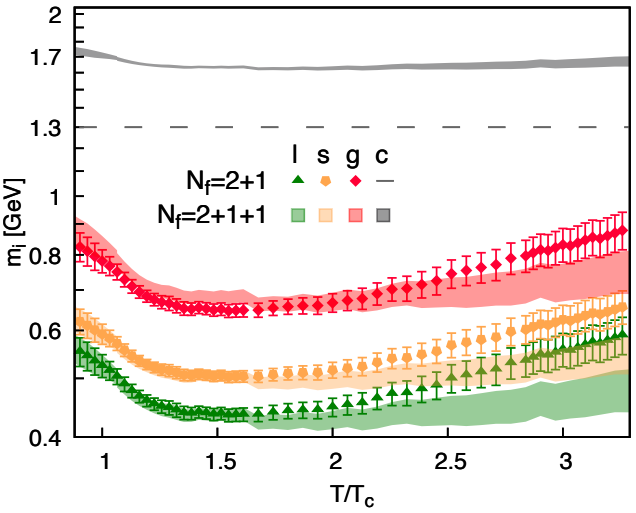


Figure 2. The quasiparticle masses $m_i(G(T), T)$, as functions of temperature T scaled by the pseudocritical value $T_c = 155$ MeV, for systems with different numbers N_f of quark flavors. In the $N_f = 2+1$ scenario, $m_c = 1.3$ GeV, as indicated, while in the $N_f = 2+1+1$, all masses are temperature-dependent (see text for details).

3. Charm Quark Evolution

Thermal production of particles can be explored in kinetic theory by solving the differential rate equation [20–22]

$$\partial_\nu (n_c\, u^\nu) = \left[2\bar{\sigma}_{l\bar{l}\to c\bar{c}} \left(\frac{1}{2} n_l^0\right)^2 + \bar{\sigma}_{s\bar{s}\to c\bar{c}} \left(n_s^0\right)^2 + \frac{1}{2}\bar{\sigma}_{gg\to c\bar{c}} \left(n_g^0\right)^2 \right] \left[1 - \left(\frac{n_c}{n_c^0}\right)^2 \right], \quad (4)$$

where n_c is the out-of-equilibrium number density of charm quarks, u^ν is the flow four-velocity, and ∂_ν is the partial derivative. The rate equation describes the evolution of n_c with time τ (or with temperature, when $T(\tau)$ is known) as a result of the microscopic

interactions within the QGP. The thermal-averaged cross sections $\bar{\sigma}_{ii'\to c\bar{c}}$ correspond to the scatterings producing the $c\bar{c}$ pairs from various quasiparticle species that are described by the equilibrium number densities,

$$n_i^0 = d_i \int \frac{d^3p}{(2\pi)^3} \left(e^{E_i/T} \pm 1\right)^{-1}, \tag{5}$$

which correspond to the Fermi–Dirac (with '+' sign for quarks) or Bose–Einstein ('−' sign for gluons) statistics; d_i are the degeneracy factors that include possible color and spin configurations: $d_l = 12$, $d_{s,c} = 6$, $d_g = 16$. The dispersion relation reads $E_i = \sqrt{p^2 + m_i^2}$, with the momentum p and the effective quasiparticle mass (1).

Note that as charm quarks become equilibrated, i.e., as n_c reaches its equilibrium value n_c^0, the right-hand side of the Equation (5) vanishes. The numerical pre-factors in Equation (4) are responsible for the appropriate counting of quark and gluon degrees of freedom [22] and are missing in the previous study [23].

This investigation focuses on the square bracket of Equation (4) known as the thermal production rate of the $c\bar{c}$ pairs [16,20,21,24],

$$R_c^{\rm gain} = \left[2\bar{\sigma}_{l\bar{l}\to c\bar{c}} \left(\frac{1}{2} n_l^0\right)^2 + \bar{\sigma}_{s\bar{s}\to c\bar{c}} \left(n_s^0\right)^2 + \frac{1}{2}\bar{\sigma}_{gg\to c\bar{c}} \left(n_g^0\right)^2\right]. \tag{6}$$

The thermal-averaged cross sections $\bar{\sigma}_{ii'\to c\bar{c}}$ are computed from the total cross sections $\sigma_{ii'\to c\bar{c}}$ according to the following prescription [25,26]:

$$\bar{\sigma}_{ii'\to c\bar{c}} = \left[8\,\frac{m_i^2}{T^2}\,\frac{m_{i'}^2}{T^2}\,K_2\left(\frac{m_i}{T}\right) K_2\left(\frac{m_{i'}}{T}\right)\right]^{-1}$$
$$\times \int_{\sqrt{s_0}}^{\infty} d\sqrt{s} \left\{\sigma_{ii'\to c\bar{c}}\, K_1\left(\frac{\sqrt{s}}{T}\right) \left[\frac{s}{T^2} - \left(\frac{m_i^2}{T^2} + \frac{m_{i'}^2}{T^2}\right)^2\right] \left[\frac{s}{T^2} - \left(\frac{m_i^2}{T^2} - \frac{m_{i'}^2}{T^2}\right)^2\right]\right\}, \tag{7}$$

where $K_{1(2)}$ are Bessel functions of the first (second) kind; $\sqrt{s}$ is the total energy of the scattering, bound from below by $\sqrt{s_0} = \max\{m_i + m_{i'}, m_c + m_{\bar{c}}\} = 2m_c$. In the QPM under consideration, the total cross sections are calculated at tree level, accounting for massive propagators of the on-shell quasiparticles [11]. Note that the Bessel functions in the expression (7) appear from the assumption that in the studied temperature range, the quasiparticles are heavy enough to be described just as well by the classical Boltzmann statistics.

The temperature dependence of the production rate of charm quarks in $N_f = 2 + 1$ has been reported earlier in Ref. [22], where the QPM results were juxtaposed to the alternative studies performed in Refs. [14,21].

To analyze the time dependence of the charm quark production rate, let us consider the QGP as a boost-invariant ideal fluid propagating longitudinally. These assumptions are associated with the so-called Bjorken flow; thus the evolution of the system is described by the Bjorken scaling solution [27]

$$T(\tau) = T_0 \left(\frac{\tau_0}{\tau}\right)^{1/3}, \tag{8}$$

where τ_0 and $T_0 \equiv T(\tau_0)$ describe the initial state of the QGP evolution, for which the parameters (a) $T_0 = 624$ MeVand $\tau_0 = 0.2$ fm [23]. To illustrate the dependence of $R_c^{\rm gain}$ (6) on the initial conditions, the following values of the parameters (b) $T_0 = 820$ MeV and $\tau_0 = 0.5$ fm are adopted as employed in Ref. [16].

It should be pointed out that for the set (a), the system reaches the pseudocritical temperature at $\tau \simeq 13$ fm, while for the set (b) this happens at $\tau \simeq 70$ fm. Such quite a long

QGP lifetime is rather disfavored by the current analyses of the experimental data [28–31], in which the freeze-out of the fireball takes place at around 10–15 fm, i.e., as in the case (a).

Figure 3 shows the production rate of charm quarks (6) as a function of time τ computed with the initial parameter cases (a) and (b) for the QGP with different numbers of quark flavors. In the case (b), following the assumptions from Ref. [16], a smaller constituent mass of charm quark is used, $m_c^{(0)} = 1.2$ GeV, which remains constant in the $N_f = 2+1$ case or becomes dressed according to Equation (1) in the $N_f = 2+1+1$ scenario.

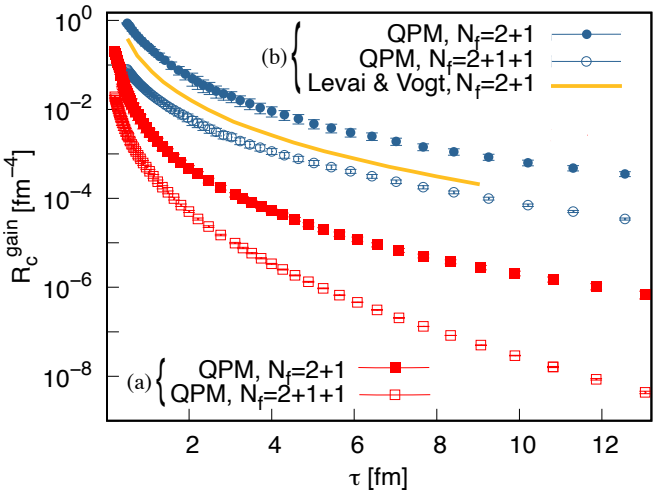


Figure 3. QPM-computed production rate R_c^{gain} of charm quarks as a function of time τ for different numbers N_f of quark flavors and the two sets of initial condition parameters: (a) $T_0 = 624$ MeV, $\tau_0 = 0.2$ fm, $m_c^{(0)} = 1.3$ GeV and (b) $T_0 = 820$ MeV, $\tau_0 = 0.5$ fm, $m_c^{(0)} = 1.2$ GeV, see text for details. The result presented in Ref. [16] for PbPb collisions at LHC is also reproduced (marked 'Levai & Vogt').

For both sets of the initial parameters, one observes that the production rate of charm quasiquarks in the $N_f = 2+1+1$ case is suppressed compared to the $N_f = 2+1$ scenario, where charm quarks are treated as impurities of constant mass. For the condition (a), a substantial difference (of approximately two orders of magnitude) appears in the crossover region, illustrating that the charm quark mass has quite an impact on the production rate computed within the QPM. The production rate is suppressed by the larger charm quark mass in the $N_f = 2+1+1$ description, which was also observed earlier for various constant masses of c-quarks employed in the dynamical quasiparticle model with $N_f = 2+1$ [24].

Comparing the results obtained for the initial parameters (b), earlier used in Ref. [16] for a parton gas of massive quasiparticles, an overall quantitative agreement is observed, since both studies employ the quasiparticle framework with $N_f = 2+1$ quark flavors. A numerical discrepancy between the studies arises from the quantitative differences of the applied couplings. Using the $G(T)$ employed in Ref. [16], the result of the latter is reproduced as shown in Figure 3. All the numerical results obtained with the set (b exceed the results computed with the set (a) due to a higher initial temperature, which reflects the sensitivity of the $c\bar{c}$ production rate to the choice of the initial parameters T_0 and τ_0.

For the initial condition (a), the discrepancy between the two curves suggests the importance of the formulation of the quasiparticle approach with properly included charm quarks, i.e., as quasiparticles. A lower value of R_c^{gain}(6) leads to a smaller number of thermally produced $c\bar{c}$ pairs. Thus, the result obtained for $N_f = 2+1+1$ is expected to provide a better quantitative agreement with the experimental data, since the analysis of the charm yield performed within the Statistical Hadronization Model (SHM) [5] suggests that

the number of charm quarks produced at the earlier stage of the heavy-ion collisions stays approximately the same after the QGP phase. A direct comparison with the experimental data requires Equation (4) to be solved, which is considered to be given elsewhere [32].

4. Conclusions

In this paper, the production rate of charm quarks has been explored by employing the quasiparticle model with various microscopic descriptions of strongly interacting matter: $N_f = 2+1$ versus $N_f = 2+1+1$ quark flavors. Moreover, different initial conditions have been tested for the evolution of the QGP described as an ideal fluid propagating in the longitudinal direction. The results obtained reveal that as soon as the charm quarks are treated as effectively dressed quasiparticles ($N_f = 2+1+1$), their thermal production rate significantly diminishes in the vicinity of the crossover, compared to the $N_f = 2+1$ scenario in which charm quarks are treated as impurities of constant mass. The observed difference suggests that the incorporation of heavy flavors as dynamical degrees of freedom might be essential in order to appropriately capture the properties of heavy flavor in the QGP described in the effective quasiparticle approaches. A closer agreement with the experimental data for the charm quark yield is expected for charm quarks considered as quasiparticles that affect the QGP thermodynamics. One also notices a continual suppression of the $c\bar{c}$ production rate for lower initial temperature of the QGP. Furthermore, for a certain initial condition, the obtained results appear in line with the production rate of charm quarks studied earlier in the alternative quasiparticle framework with $N_f = 2+1$ [16].

Funding: This research was funded by the Polish National Science Center (NCN) under the PRELUDIUM 20 Grant No. UMO-2021/41/N/ST2/02615.

Data Availability Statement: The data presented in this study are available on request from the corresponding author.

Acknowledgments: The author would like to thank Pasi Huovinen, Chihiro Sasaki and Krzysztof Redlich for inspiring discussions and useful comments.

Conflicts of Interest: The author declares no conflicts of interest.

References

1. Das, S.K.; Torres-Rincon, J.M.; Rapp, R. Charm and bottom hadrons in hot hadronic matter. *Phys. Rep.* **2025**, *1129–1131*, 1–53. [CrossRef]
2. Adam, J. et al. [STAR Collaboration] Centrality and transverse momentum dependence of D^0-meson production at mid-rapidity in Au + Au collisions at $\sqrt{s_{NN}} = 200$ GeV. *Phys. Rev. C* **2019**, *99*, 034908. [CrossRef]
3. Acharya, S. et al. [ALICE Collaboration] The ALICE experiment: A journey through QCD. *Eur. Phys. J. C* **2024**, *84*, 813. [CrossRef]
4. Tumasyan, A. et al. [The CMS Collaboration] Study of charm hadronization with prompt Λ_c^+ baryons in proton–proton and lead–lead collisions at $\sqrt{s_{\mathrm{NN}}}$ = 5.02 TeV. *J. High Energy Phys.* **2024**, *2024*, 128. [CrossRef]
5. Andronic, A.; Braun-Munzinger, P.; Köhler, M.K.; Mazeliauskas, A.; Redlich, K.; Stachel, J.; Vislavicius, V. The multiple-charm hierarchy in the statistical hadronization model. *J. High Energy Phys.* **2021**, *2021*, 35. [CrossRef]
6. Apolinário, L.; Lee, Y.-J.; Winn, M. Heavy quarks and jets as probes of the QGP. *Prog. Part. Nucl. Phys.* **2022**, *127*, 103990. [CrossRef]
7. Capellino, F.; Dubla, A.; Floerchinger, S.; Grossi, E.; Kirchner, A.; Masciocchi, S. Fluid dynamics of charm quarks in the quark–gluon plasma. *Phys. Rev. D* **2023**, *108*, 116011. [CrossRef]
8. Zhao, J.; Aichelin, J.; Gossiaux, P.B.; Beraudo, A.; Cao, S.; Fan, W.; He, M.; Minissale, V.; Song, T.; Vitev, I.; et al. Hadronization of heavy quarks. *Phys. Rev. C* **2024**, *109*, 054912. [CrossRef]
9. Altenkort, L. et al. [HotQCD Collaboration] Quark mass dependence of heavy quark diffusion coefficient from lattice QCD. *Phys. Rev. Lett.* **2024**, *132*, 051902. [CrossRef]
10. Andronic, A.; Gossiaux, P.B.; Petreczky, P.; Rapp, R.; Strickland, M.; Blaizot, J.P.; Brambilla, N.; Braun-Munzinger, P.; Chen, B.; Delorme, S.; et al. Comparative study of quarkonium transport in hot QCD matter. *Eur. Phys. J. A* **2024**, *60*, 88. [CrossRef]

11. Mykhaylova, V.; Bluhm, M.; Redlich, K.; Sasaki, C. Quark-flavor dependence of the shear viscosity in a quasiparticle model. *Phys. Rev. D* **2019**, *100*, 034002. [CrossRef]
12. Mykhaylova, V.; Sasaki, C. Impact of quark quasiparticles on transport coefficients in hot QCD. *Phys. Rev. D* **2021**, *103*, 014007. [CrossRef]
13. Auvinen, J.; Eskola, K.J.; Huovinen, P.; Niemi, H.; Paatelainen, R.; Petreczky, P. Temperature dependence of η/s of strongly interacting matter: Effects of the equation of state and the parametric form of $(\eta/s)(T)$. *Phys. Rev. C* **2020**, *102*, 044911. [CrossRef]
14. Song, T.; Grishmanovskii, I.; Soloveva, O.; Bratkovskaya, E. Thermal production of charm quarks in relativistic heavy-ion collisions. *Phys. Rev. C* **2024**, *110*, 034906. [CrossRef]
15. Sambataro, M.L.; Greco, V.; Parisi, G.; Plumari, S. Quasi particle model vs lattice QCD thermodynamics: Extension to $N_f = 2+1+1$ flavors and momentum dependent quark masses. *Eur. Phys. J. C* **2024**, *84*, 881. [CrossRef]
16. Levai, P.; Vogt, R. Thermal charm production by massive gluons and quarks. *Phys. Rev. C* **1997**, *56*, 2707–2717. [CrossRef]
17. Pisarski, R.D. Renormalized fermion propagator in hot gauge theories. *Nucl. Phys. A* **1989**, *498*, 423c–428c. [CrossRef]
18. Borsányi, S.; Fodor, Z.; Hoelbling, C.; Katz, S.D.; Krieg, S.; Szabó, K.K. Full result for the QCD equation of state with $2+1$ flavors. *Phys. Lett. B* **2014**, *730*, 99–104. [CrossRef]
19. Borsányi, S.; Fodor, Z.; Guenther, J.; Kampert, K.H.; Katz, S.D.; Kawanai, T.; Kovacs, T.G.; Mages, S.W.; Pasztor, A.; Pittler, F.; et al. Calculation of the axion mass based on high-temperature lattice quantum chromodynamics. *Nature* **2016**, *539*, 69–71. [CrossRef]
20. Biró, T.S.; van Doorn, E.; Müller, B.; Thoma, M.H.; Wang, X.-N. Parton equilibration in relativistic heavy ion collisions. *Phys. Rev. C* **1993**, *48*, 1275–1284. [CrossRef]
21. Zhang, B.-W.; Ko, C.M.; Liu, W. Thermal charm production in a quark–gluon plasma in Pb–Pb collisions at $\sqrt{s_{NN}} = 5.5$ TeV. *Phys. Rev. C* **2008**, *77*, 024901. [CrossRef]
22. Mykhaylova, V. Reviewing the production rate of charm quarks in effective kinetic theory. *J. Subat. Part. Cosmol.* **2025**, *3*, 100031. [CrossRef]
23. Mykhaylova, V. Production rate of charm quarks in the quasiparticle approach. *Acta Phys. Polon. Suppl.* **2024**, *17*, 6-A10. [CrossRef]
24. Song, T.; Zhao, J.; Grishmanovskii, I. Heavy quark potential and thermal charm production in heavy-ion collisions. *arXiv* **2024**, arXiv:2411.07383. [CrossRef]
25. Braun-Munzinger, P.; Redlich, K. Charmonium production from the secondary collisions at LHC energy. *Eur. Phys. J. C* **2000**, *16*, 519–525. [CrossRef]
26. Kadam, G.P.; Mishra, H. Dissipative properties of hot and dense hadronic matter in an excluded-volume hadron resonance gas model. *Phys. Rev. C* **2015**, *92*, 035203. [CrossRef]
27. Bjorken, J.D. Highly relativistic nucleus–nucleus collisions: The central rapidity region. *Phys. Rev. D* **1983**, *27*, 140–151. [CrossRef]
28. Shou, Q.-Y.; Ma, Y.-G.; Zhang, S.; Zhu, J.-H.; Mao, Y.-X.; Pei, H.; Yin, Z.-B.; Zhang, X.-M.; Zhou, D.-C.; Peng, X.-Y.; et al. Properties of QCD matter: A review of selected results from ALICE experiment. *Nucl. Sci. Tech.* **2024**, *35*, 219. [CrossRef]
29. Sinyukov, Y.M.; Shapoval, V.; Adzhymambetov, M. Space–time structure of particle emission and femtoscopy scales in ultrarelativistic heavy-ion collisions. *Universe* **2023**, *9*, 433. [CrossRef]
30. Kasza, G.; Csörgő, T. Lifetime estimations from RHIC Au + Au data. *Int. J. Mod. Phys. A* **2019**, *34*, 1950147. [CrossRef]
31. Cimerman, J.; Karpenko, I.; Tomášik, B.; Huovinen, P. Next-generation multifluid hydrodynamic model for nuclear collisions at $\sqrt{s_{NN}}$ from a few GeV to a hundred GeV. *Phys. Rev. C* **2023**, *107*, 044902. [CrossRef]
32. Mykhaylova, V.; Redlich, K.; Sasaki, C. Charm Quark Kinetics in Heavy-Ion Collisions. Unpublished work, 2025.

Disclaimer/Publisher's Note: The statements, opinions and data contained in all publications are solely those of the individual author(s) and contributor(s) and not of MDPI and/or the editor(s). MDPI and/or the editor(s) disclaim responsibility for any injury to people or property resulting from any ideas, methods, instructions or products referred to in the content.